Supplement of Atmos. Chem. Phys., 26, 3783–3803, 2026
https://doi.org/10.5194/acp-26-3783-2026-supplement

Atmospheric Chemistry and Physics
Open Access
EGU

Supplement of

Global NO_2 changes between 2019 and 2024 as observed by TROPOMI in urban areas and emerging hotspots

Daniel E. Huber et al.

Correspondence to: Daniel E. Huber (daniel.huber@gwu.edu)

S1 Sensitivity of Urban Background NO_2 VCDs

To estimate the background NO_2 vertical column density (VCD) for each GHS-SMOD city and for each year, we adopted a percentile-based approach applied to gridded annual mean TROPOMI NO_2 data (0.1° × 0.1°). For each of the 11,534 urban clusters defined by the GHS-SMOD dataset, we first subset the global NO_2 field to include all grid cells extending 0.5° beyond the northernmost, southernmost, easternmost, and westernmost points of each city's boundary. This local subset captures the surrounding area from which the city-specific background is calculated.

Within this subset, we evaluated several percentile thresholds (10th, 50th, 60th, 70th, and 75th percentiles) to characterize the spatial distribution of grid cells with NO_2 concentrations that are either above or below a city's background NO_2 value (Figs. S1-S4). Across most cities, the 50th-percentile value provides a spatially-consistent estimate of the background, including a buffer zone surrounding the majority of urban boundaries. For a handful of larger cities, NO_2 at the 50th percentile occasionally overlaps with portions of the urban core (Fig S1b), and for some smaller cities, using the 50th percentile occasionally results in a larger buffer. Despite this, using this method offers a uniform metric that can be applied consistently across the more than 11,000 GHS-SMOD urban clusters.

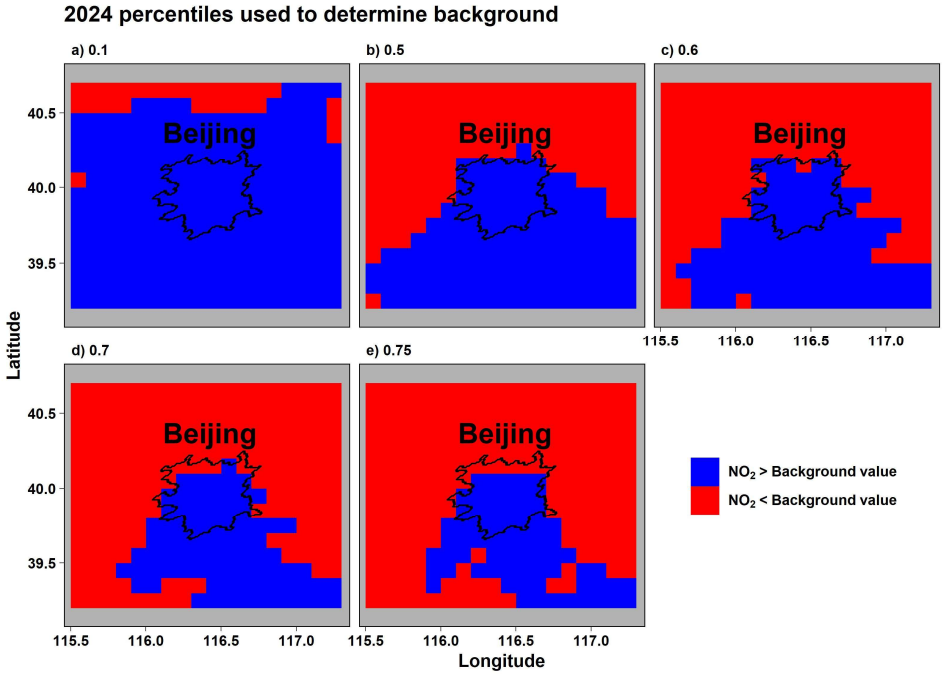

Figure S1: Evaluation of percentile thresholds applied to 2024 mean TROPOMI NO_2 VCDs to determine the 2024 background for Beijing, China when using the following percentiles: (a) 10th, (b) 50th, (c) 60th, (d) 70th, (e) 75th.

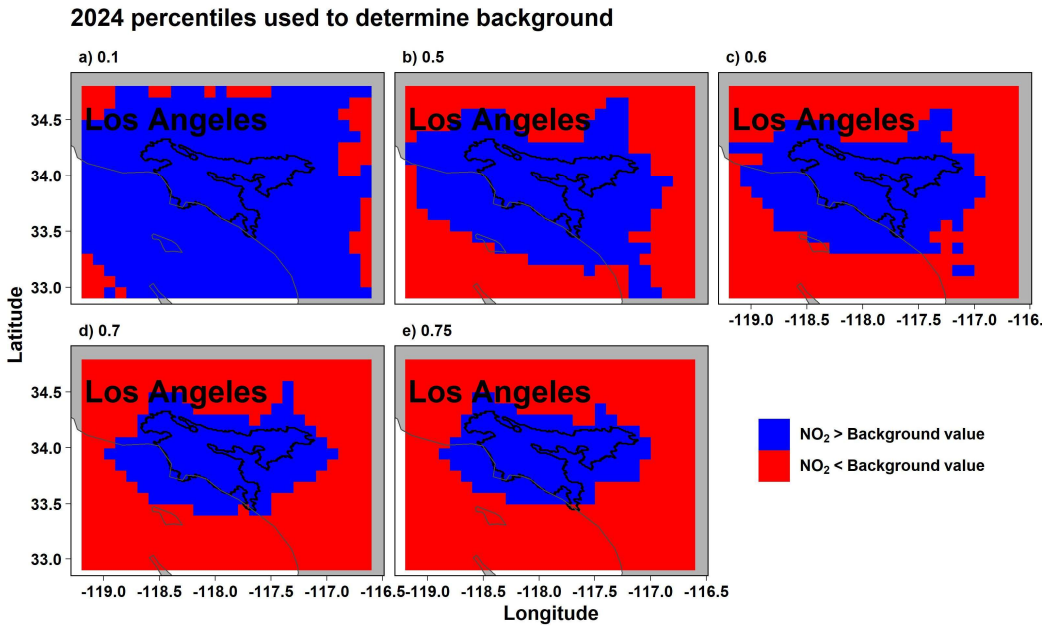

20

21 **Figure S2: Same as Fig. S1, but an example for Los Angeles, U.S. in 2024.**

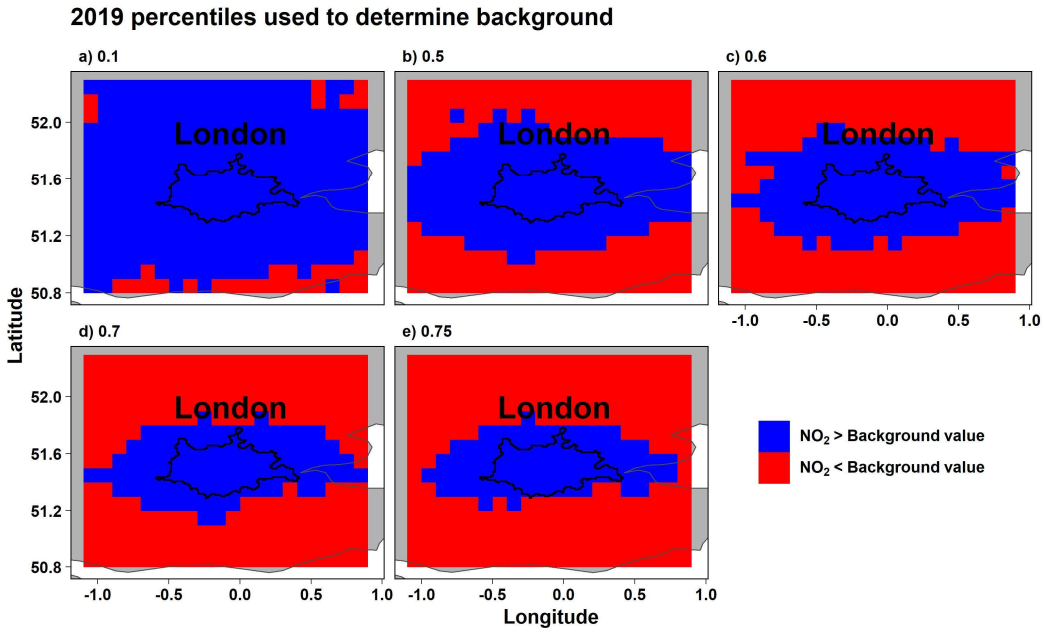

22

23 **Figure S3: Same as Fig. S1, but an example for London, U.K. in 2019.**

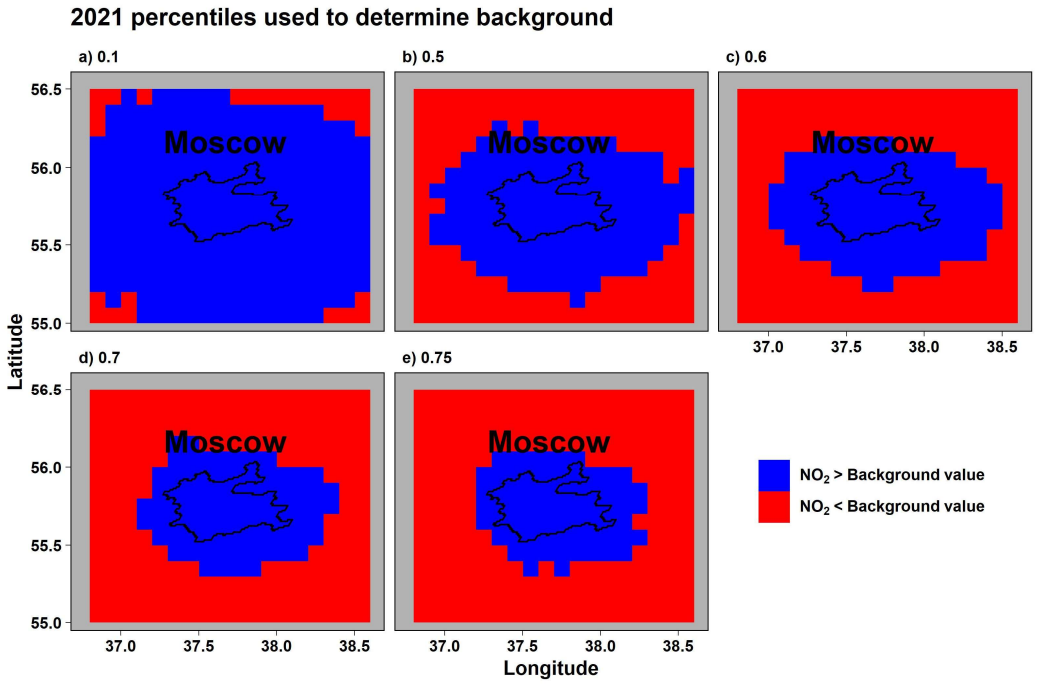

Figure S4: Same as Fig. S1, but an example for Moscow, Russia in 2021.

Sensitivity analyses demonstrate that the choice of percentile has only a modest influence on the results from this work (Fig. S5-S6). While the population-weighted background concentration aggregated to the continent level value does vary when using background NO_2 at each city's percentiles (Fig. S5), the influence that this has on urban VCD enhancement (VCD_{ENH}) calculations remains very minimal (Fig. S6). Panel e on Figures 6-11 within the manuscript are therefore only minimally influenced by the choice of percentile. The resulting city-level VCD_{ENH} magnitudes and interannual variations changed by less than 5% for most continents, with the most variability observed in Africa. The background fields were also found to be spatially coherent among adjacent cities (Fig. S7), typically differing by less than $\pm 0.2 \times 10^{15}$ molecules cm^{-2}, consistent with expectations for shared regional backgrounds. Overall, this percentile-based framework provides a transparent, scalable, and globally consistent method for estimating NO_2background levels. The sensitivity tests and cross-city comparisons confirm that the main findings are robust to reasonable variations in the background definition.

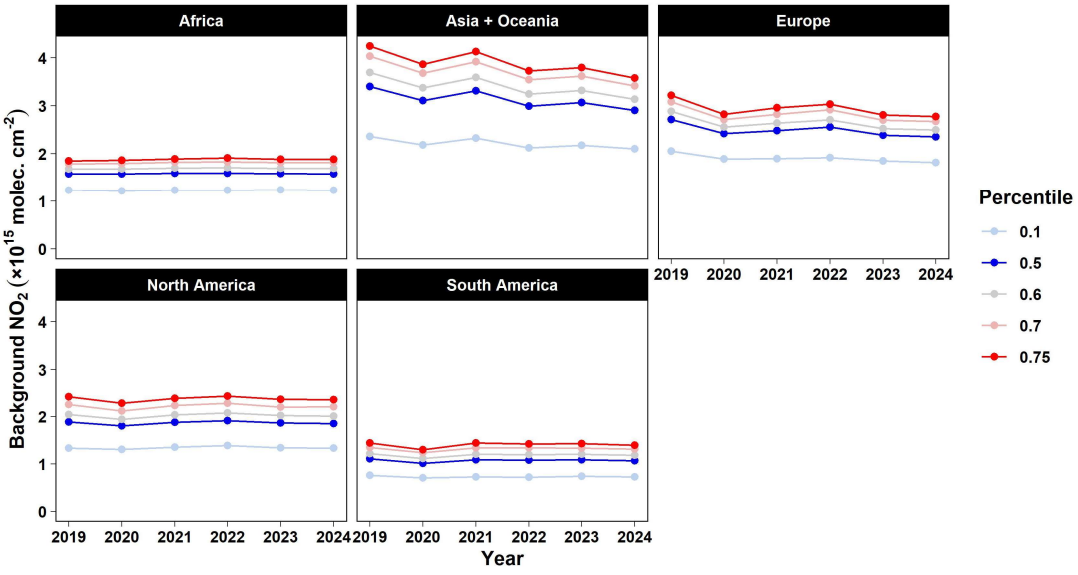

Figure S5: Population-weighted background NO_2 VCDs for each continent and when using different percentile thresholds for each city.

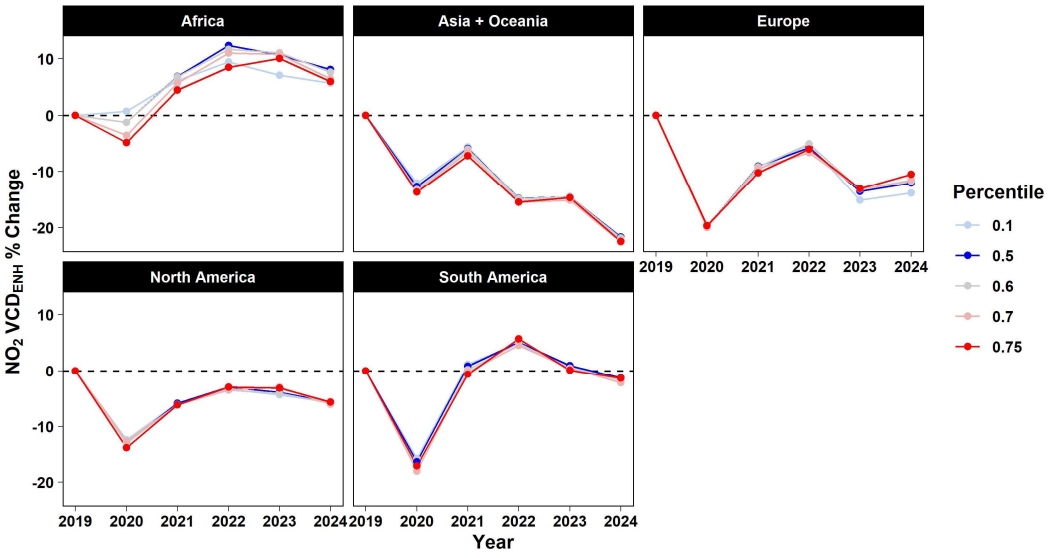

Figure S6: Percent change in population-weighted VCD enhancement (VCD_{ENH}) for each continent and when using different percentile thresholds for background concentrations for each city.

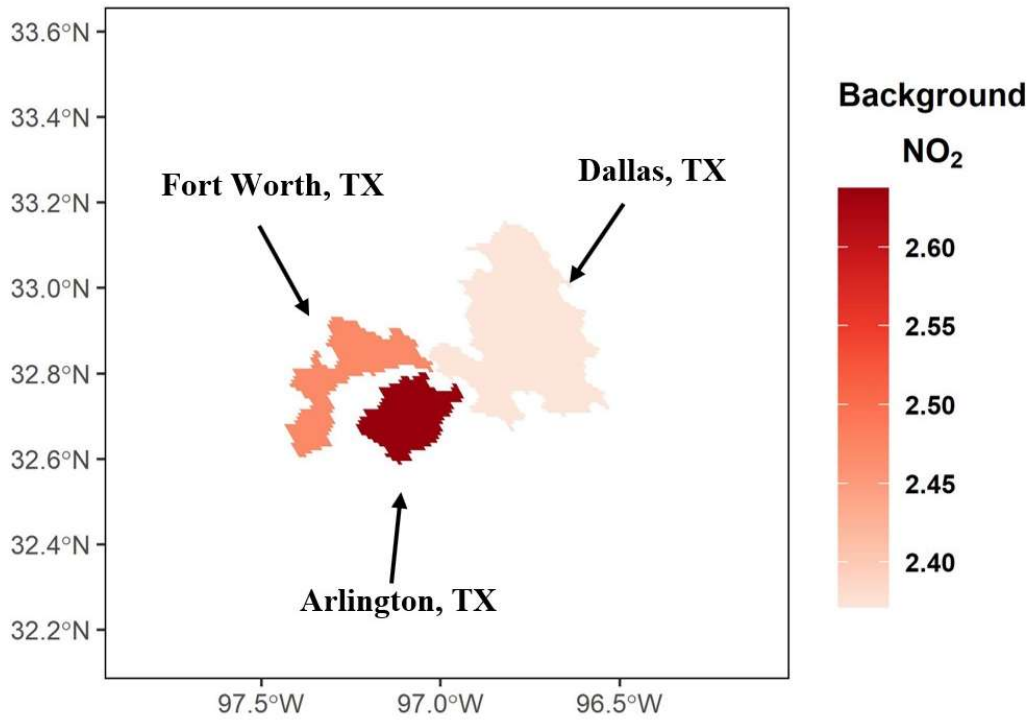

Figure S7: Background NO_2 VCDs for three adjacent GHS-SMOD urban clusters in the Dallas-Fort Worth urban region: Fort Worth, TX (left), Arlington, TX (middle), and Dallas, TX (right).

S2 Additional Supplementary Figures

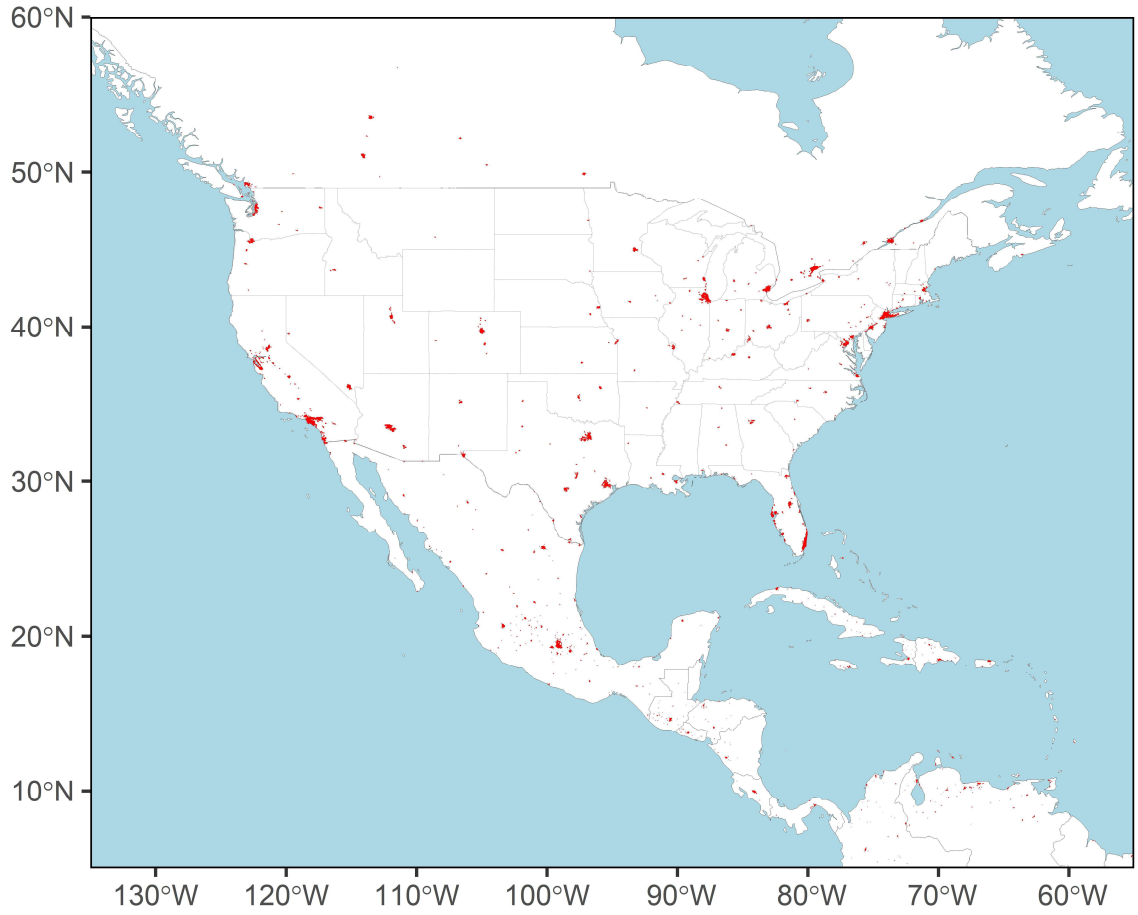

Figure S8: Spatial representation of all urban clusters included in the 2023a version of GHS-SMOD (red polygons), zoomed on North America.

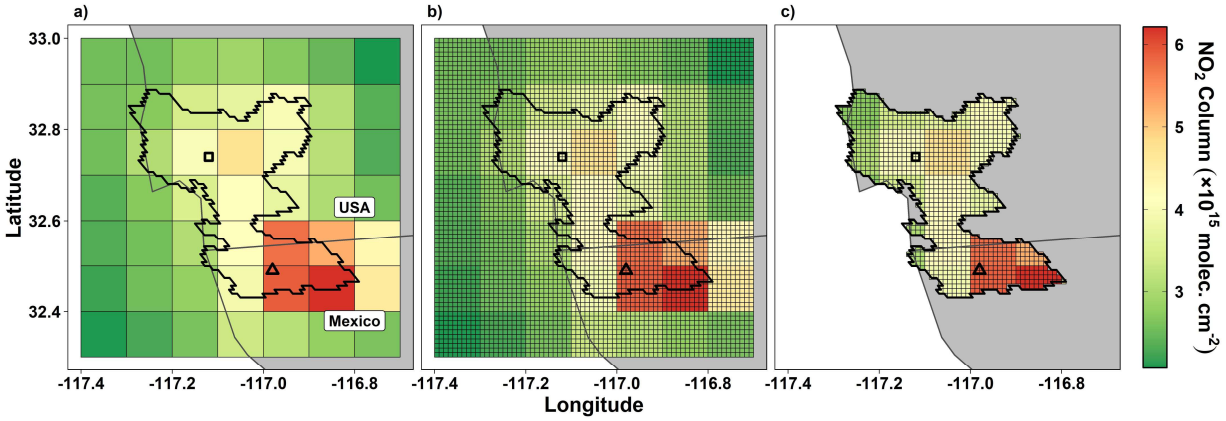

Figure S9: Spatial representation of one urban cluster boundary from the version 2023a GHS-SMOD dataset (black outline) that encompasses both San Diego, CA, USA (black square) and Tijuana,

Mexico (black triangle). Colors show TROPOMI tropospheric NO_2 column concentrations (a) at the 0.1 × 0.1 degree spatial resolution of the oversampled level 3 product, (b) after disaggregating to 0.01 × 0.01 degrees and (c) after subsetting for grid cells within the urban cluster boundary, which are subsequently used to determine average NO_2 concentrations for each urban cluster.

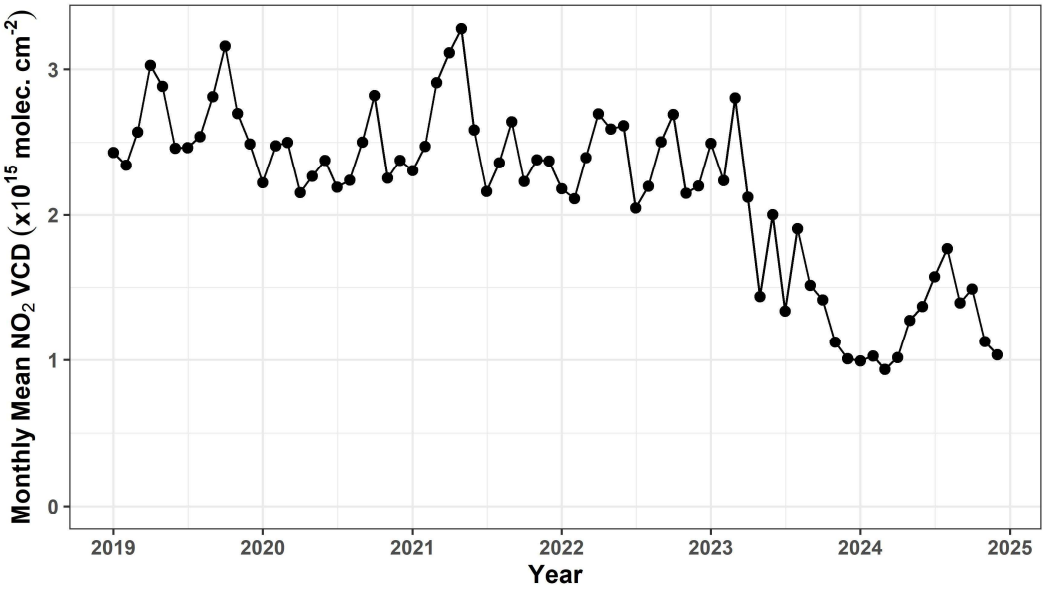

Figure S10: Monthly mean NO_2 VCD for the Khartoum, Sudan urban cluster.

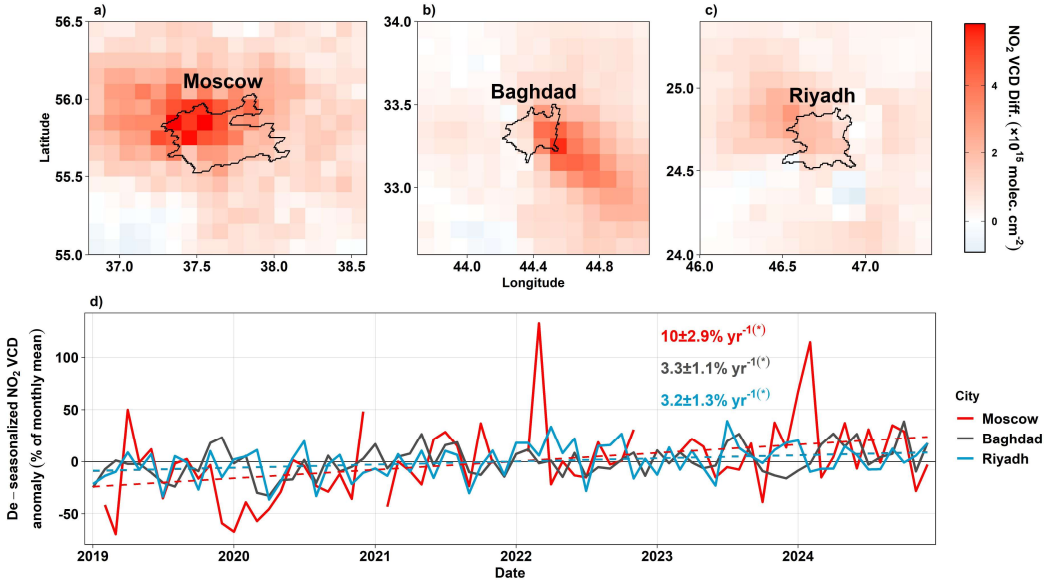

Figure S11: Absolute change in NO_2 VCD from 2019 to 2024 for three U.S. cities: (a) Moscow, Russia; (b) Baghdad, Iraq; and (c) Riyadh, Saudi Arabia. Colors in panels a-c show VCD change, thin lines show national and state borders or coastlines, and thick lines show the GHS-SMOD urban boundary. (d) Solid lines show de-seasonalized monthly VCD anomaly from 01/2019 through

12/2024, colored by city. Dashed lines are produced from ordinary least-squares regression. The % change yr^{-1}, standard error and statistical significance is reported in the top right of panel d.

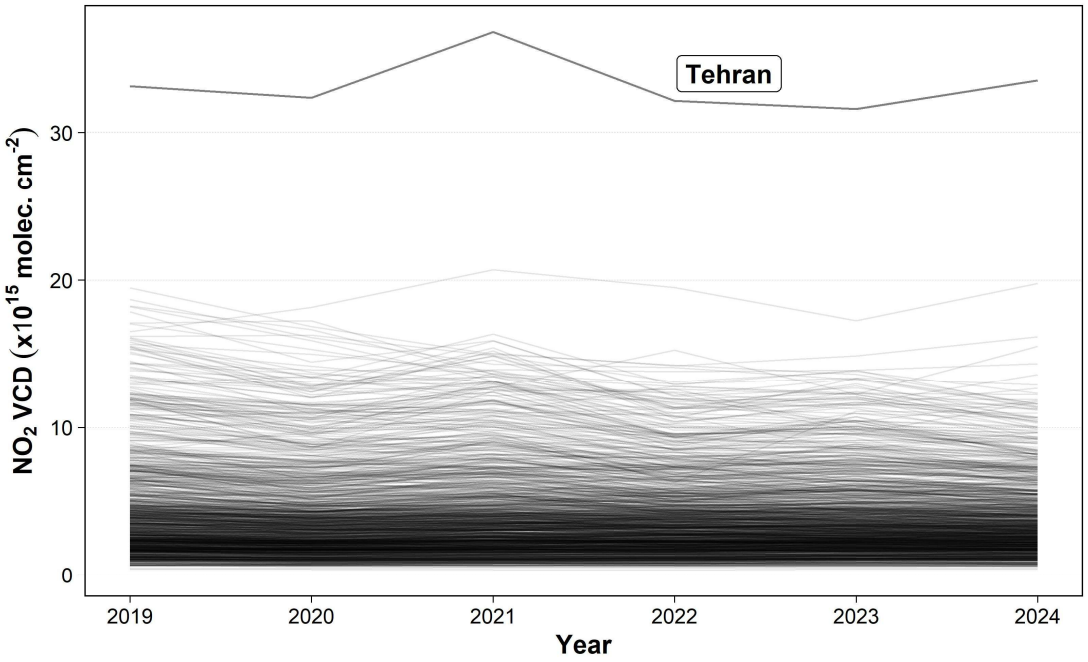

Figure S12: Annual mean TROPOMI NO_2 VCD for all GHS-SMOD urban clusters with a population greater than 500,000 (thin gray lines) and for the Tehran, Iran urban cluster (thick gray line).

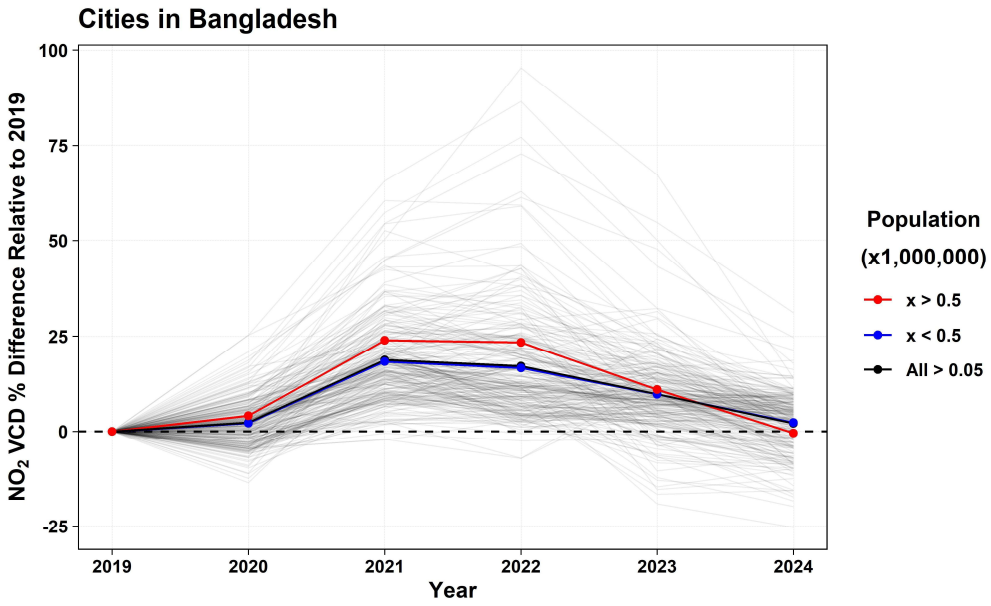

79

80 **Figure S13: Annual mean TROPOMI NO_2 VCD for individual GHS-SMOD cities in Bangladesh**
81 **(gray lines) and averages for all cities (black), cities with population < 500,000 (blue) and > 500,000**
82 **(red).**

83

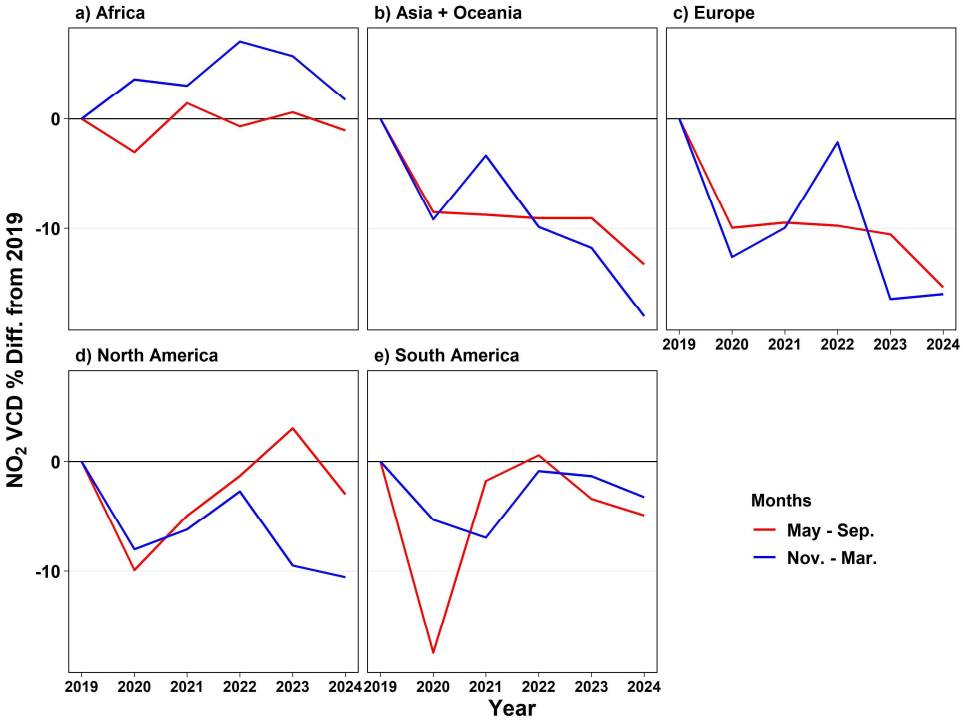

84

85 **Figure S14: Relative change in urban population-weighted NO_2 VCDs from 2019 to 2024 for May –**
86 **September (red lines) and November – March (blue lines) in (a) Africa, (b) Asia and Oceania, (c)**
87 **Europe, (d) North America and (e) South America.**

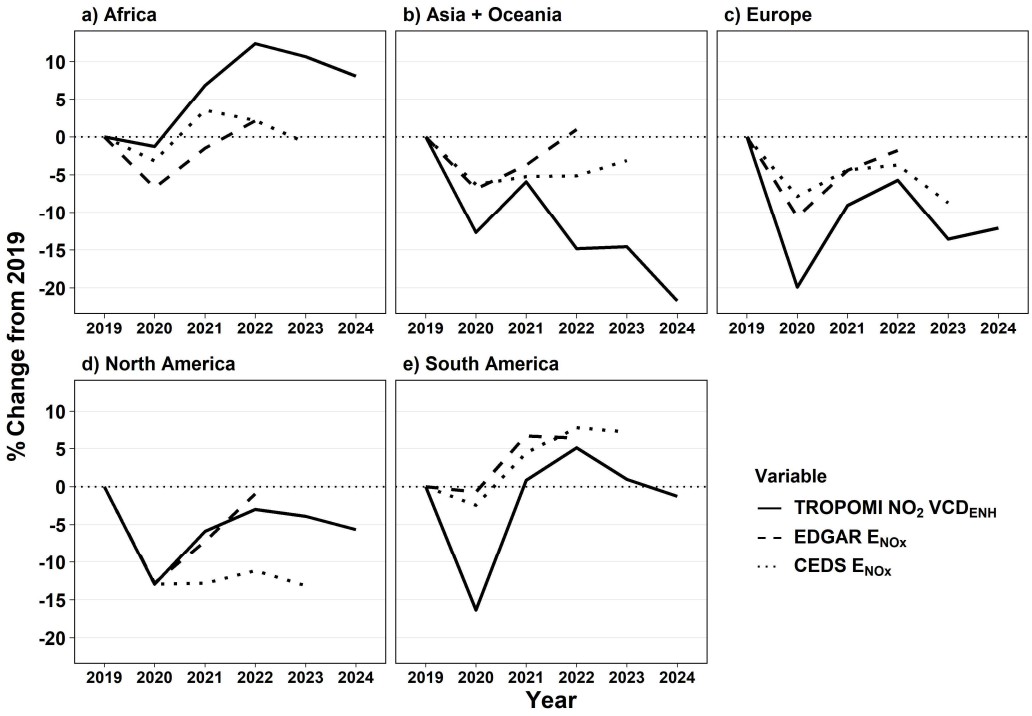

Figure S15: Relative change in urban population-weighted VCD_{ENH} (solid line; 2019-2024), EDGAR NOx emissions (dashed line; 2019-2022) and CEDS NOx emissions (dotted line; 2019-2023) in (a) Africa, (b) Asia and Oceania, (c) Europe, (d) North America and (e) South America.

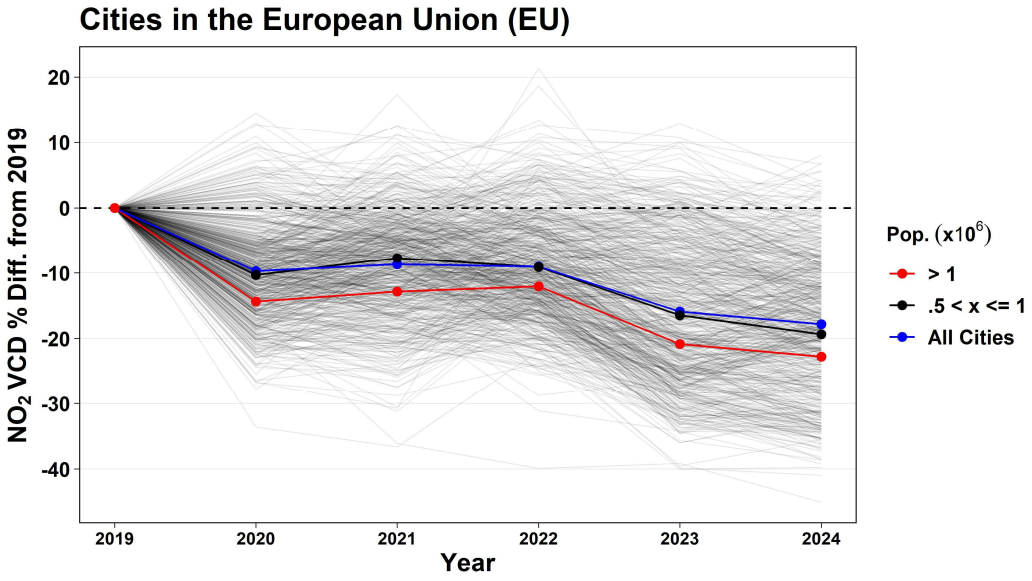

Figure S16: Annual mean TROPOMI NO_2 VCD for individual GHS-SMOD cities in the E.U. (gray lines) and averages for all cities (blue), cities with population < 1 million (black) and > 1 million (red).

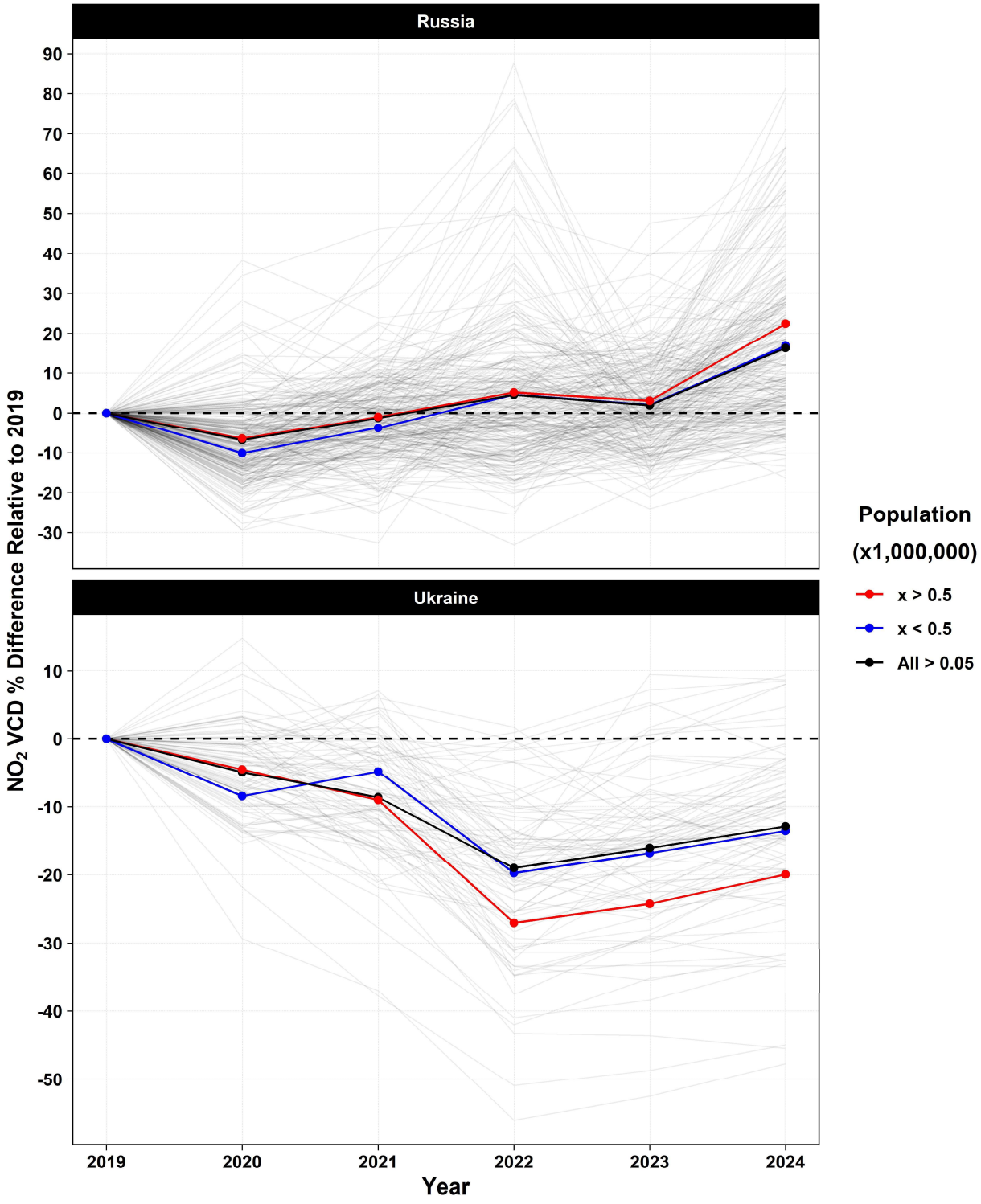

Figure S17: Annual mean TROPOMI NO_2 VCD for individual GHS-SMOD cities in (a) Russia and (b) Ukraine (gray lines) and averages for all cities (black), cities with population < 500,000 (blue) and > 500,000 (red).

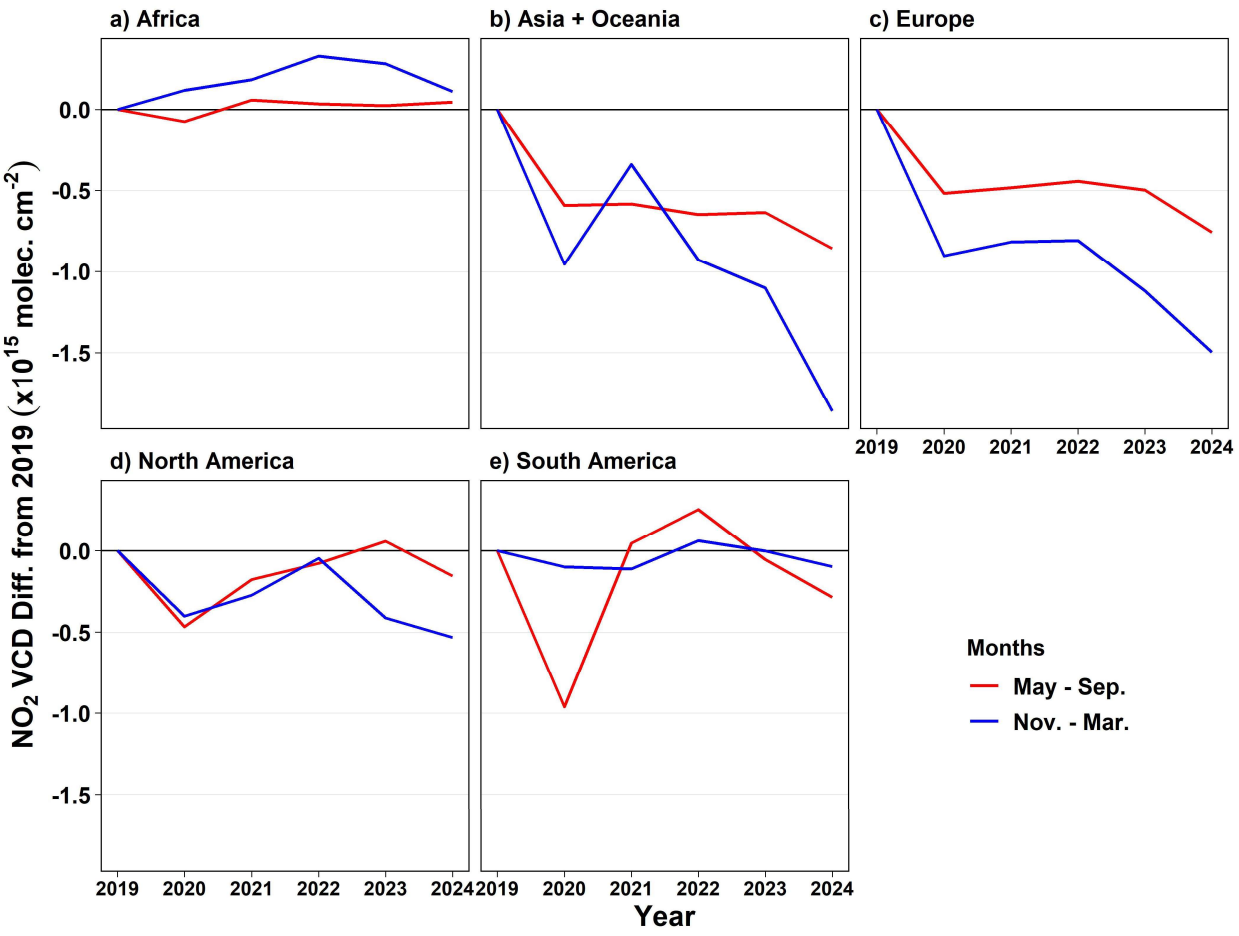

103

104 **Figure S18: Absolute population-weighted difference in VCD for urban clusters in (a) Africa, (b)**
105 **Asia and Oceania, (c) Europe, (d) North America and (e) South America for May-September (red**
106 **line) and November to March (blue line), with Russian cities removed from the analysis.**

107

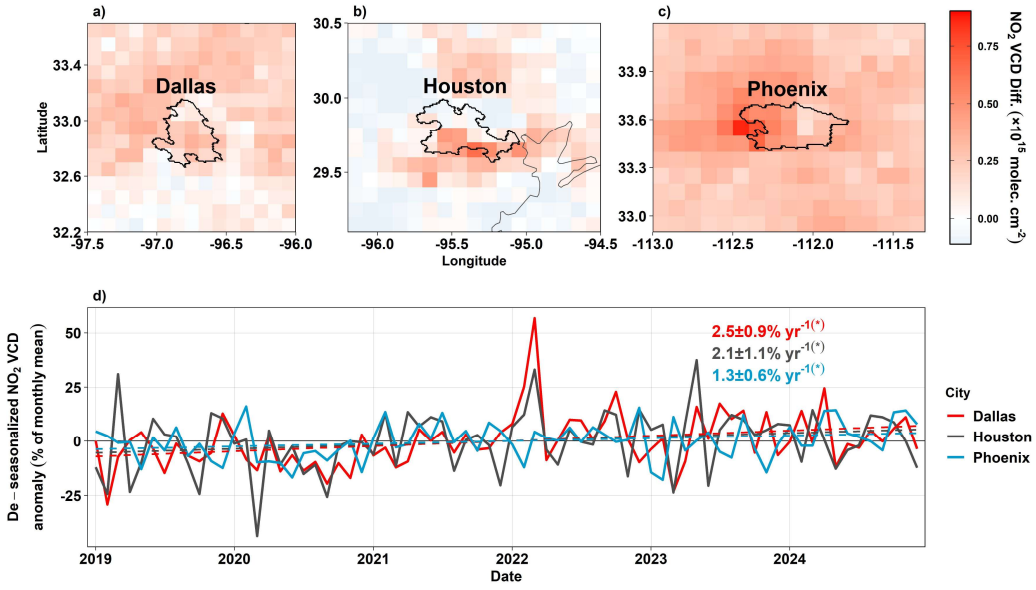

Figure S19: Same as Fig. S11, but for (a) Dallas, Texas; (b) Houston, Texas; (c) Phoenix, Arizona and (d) monthly time series.

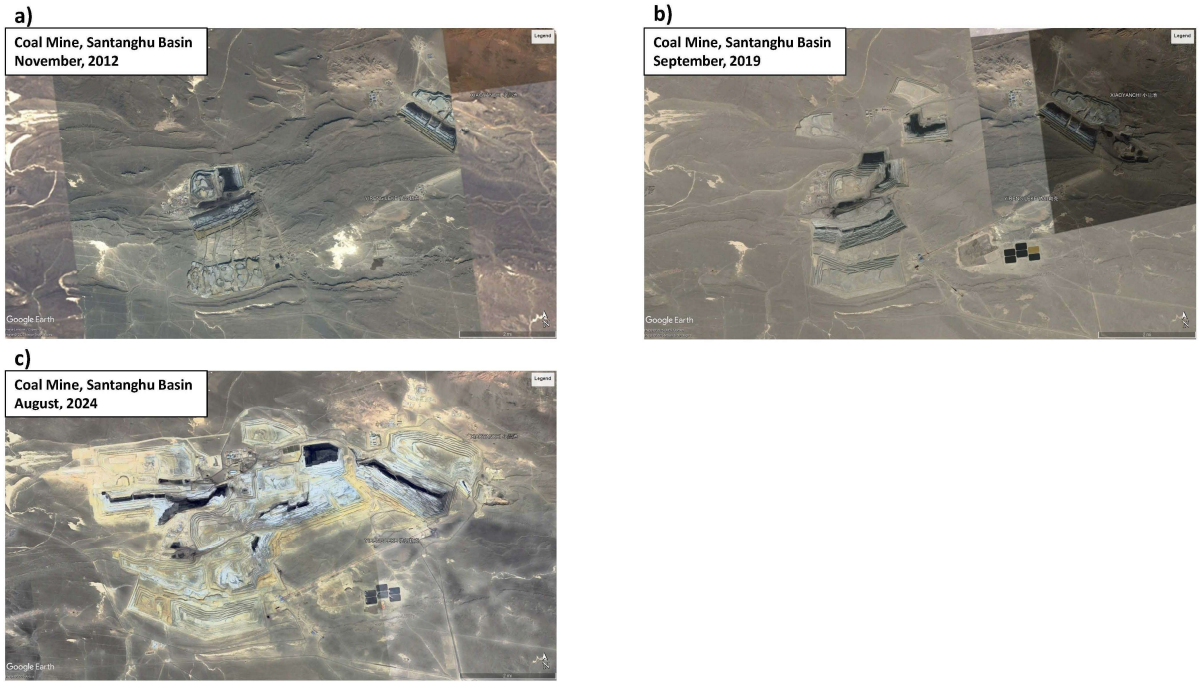

Figure S20: Satellite imagery showing the expansion of mining operations at a site in the Santanghu Basin in Xinjiang Province, China. Panels show the mine in (a) 2012, (b) 2019 and (c) 2024. Scale on the bottom right of each panel shows distance of 2 miles on the image. Imagery: (a) Copernicus/Landsat and © 2025 Maxar Technologies; (b) © 2025 CNES/Airbus and © 2025 Maxar Technologies; (c) © 2025 Maxar Technologies. Map data © 2025 Google.